PERGAMON

International Journal of Heat and Mass Transfer 42 (1999) 1597–1615

International Journal of HEAT and MASS TRANSFER

Heat transfer coefficient and friction factor correlations for the transitional flow regime in rib-roughened rectangular ducts

R. Karwa[a,*], S.C. Solanki[b], J.S. Saini[b]

[a] *Department of Mechanical Engineering, Faculty of Engineering, Jai Narain Vyas University, Jodhpur 342 011, India*
[b] *Department of Mechanical and Industrial Engineering, University of Roorkee, Roorkee 247 667, India*

Received 26 December 1995; in final form 30 July 1998

Abstract

This paper presents results of an experimental investigation of heat transfer and friction for the flow of air in rectangular ducts with repeated chamfered rib-roughness on one broad wall. The aspect ratios of the rectangular duct investigated are 4.8, 6.1, 7.8, 9.66 and 12.0. The roughened wall is uniformly heated while the remaining three walls are insulated. These boundary conditions correspond closely to those found in solar air heaters. The range of parameters studied are: Reynolds numbers from 3000 to 20 000; relative roughness heights from 0.0141 to 0.0328; the relative roughness pitch of 4.5, 5.8, 7.0 and 8.5; and rib chamfer angles of -15, 0, 5, 10, 15 and 18°. The roughness Reynolds numbers corresponding to these parameters range from 5 to 60. Friction factor and heat transfer coefficient correlations have been developed based on the law of wall similarity and heat-momentum transfer analogy.

Nomenclature

A actual heat transfer surface area [m^2]
A_s smooth plate heat transfer area [m^2]
C_p specific heat [J kg^{-1} K^{-1}]
D inside diameter [m]
D_h channel hydraulic diameter $= 4WH/\{2(W+H)\}$ [m]
e rib height [m]
e/D, e/D_h relative roughness height
e^+ roughness Reynolds number, equation (2)
f fanning friction factor
g heat transfer function (g-function), equation (5)
G mass velocity [kg s^{-1} m^{-2}]
h heat transfer coefficient [W m^{-2} K^{-1}]
H duct depth [m]
k thermal conductivity of air [W m^{-1} K^{-1}]
L test section length [m]
m mass flow rate [kg s^{-1}]
Nu Nusselt number, hD_h/k
p rib pitch [m]
p/e relative roughness pitch
Pr Prandtl number $\mu C_p/k$
Qu heat transfer rate [W]
R roughness function, equation (1)
Re Reynolds number, GD_h/μ
St Stanton number, $Nu/Re\,Pr$
T_f air temperature [°C]
T_{fm} bulk mean air temperature $= (T_o+T_i)/2$ [°C]
T_i air inlet temperature [°C]
T_o air outlet temperature [°C]
T_{pm} mean plate temperature [°C]
w rib width [m]
w/e rib width to height ratio
W duct width [m]
W/H channel aspect ratio
X length in axial direction [m].

Greek symbols

α rib angle of attack [°]
δp pressure drop in the duct [Pa]
μ dynamic viscosity [Pa s]
ρ density of air [kg m^{-3}]
ϕ chamfer angle [°].

Subscript

s smooth duct.

* Corresponding author

0017–9310/98/$ - see front matter
PII: S0017–9310(98)00252–X

1. Introduction

The use of artificial roughness on the heat transfer surface is one of the several heat transfer enhancement methods employed in advanced turbine blade cooling designs and solar air heaters.

Several experimental studies of heat transfer and friction characteristics have been carried out [1–18] for single-phase flow in roughened tubes, annuli and ducts. Mass transfer [11, 20], flow visualization techniques [11] and holographic interferometry [8, 16, 22] have been used to study the flow patterns. Most of these investigations are related to tubes, annuli, and ducts with two opposite roughened walls and with all the four walls heated. In solar air heaters, one broad wall of the rectangular section air flow passage is subjected to uniform heat flux (solar insolation) while the remaining three walls are insulated. Sparrow and Tao [20] made mass transfer study with one or two rodded walls. Sparrow and Hossfeld [15] carried out studies on rectangular duct with corrugated walls, Liu et al. [21] with pin fins on heated wall, Prasad and Saini [12] and Gupta et al. [1] with protrusion wire roughness on the heated wall. Williams et al. [10] reported improvement of thermal performance with chamfering of closely spaced repeated rectangular ribs for the flow through a circular annulus. Williams and Watts [11] investigated the friction and heat transfer characteristics of square, chamfered and wedge type repeated rib roughness ($p/e = 1.4$–8.5) for the circular annulus configuration. They [11] also studied photographically the fluid flow patterns on large scale models of these rib shapes and obtained distributions of heat transfer coefficient using mass transfer technique. These investigators [10, 11] reported the performance improvement of the order of 20–30% for chamfered rib roughness over the square and wedge type rib roughnesses.

The objective of the present experimental investigation was to generate friction and heat transfer data pertinent to heating of air in a rectangular duct with integral rectangular and chamfered repeated rib-roughness on one broad wall subject to uniform heat flux because the literature survey reveals that no serious effort has been directed towards the investigations of such nature. Table 1 gives the range of roughness and flow parameters covered in the present study and Fig. 1 shows the rib geometry investigated.

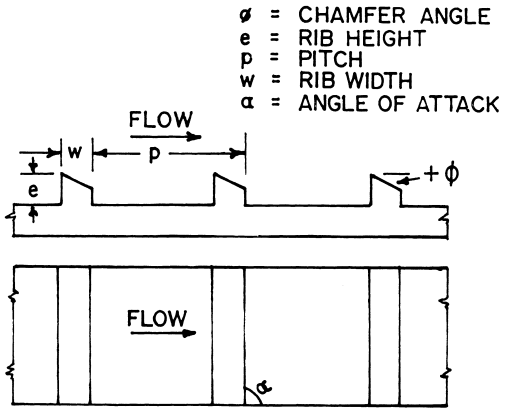

Fig. 1. Rib geometry.

The results of the present investigation have been employed to develop correlations of the roughness and heat transfer functions.

2. Rough surface analysis

The experimental results of heat transfer and fluid flow characteristics in roughened ducts have been presented either in the form of direct dependence of friction factors and heat transfer coefficients on the system and operating parameters or in the form of interrelated roughness and heat transfer functions. This later method makes it possible to present results in a most general form taking into account the various parameters involved, including the roughness parameters.

The friction correlation is based on the law of wall similarity employed by Nikuradse [2] for sand grain roughness in pipes. Nikuradse presented the pressure drop results in terms of roughness function R and roughness Reynolds number e^+. These functions have been presented as

Table 1
Experimental conditions

Reynolds number, Re	3000–20 000
Channel aspect ratio, W/H	4.8, 6.1, 7.75, 9.66, 12.0
Test length to hydraulic diameter ratio of duct, L/D_h	32, 66
Relative roughness height, e/D_h	0.014, 0.0176, 0.021, 0.027, 0.032
Relative roughness pitch, p/e	4.5, 5.8, 7.0, 8.5
Rib head chamfer angle, ϕ	-15, 0, 5, 10, 15, 18°

$$R = \sqrt{2/f} + 2.5\ln(2e/D_h) + E \quad (1)$$

and

$$e^+ = \sqrt{f/2}\, Re(e/D_h). \quad (2)$$

The constant E in equation (1) is termed as a geometric parameter dependent on the configuration of the duct. Nikuradse reported a value of this parameter as 3.75 for pipes and the same value was used by Dipprey and Sabersky [9]. However there is no general agreement on the value of E.

Nikuradse found three flow regions, namely:

(1) Hydraulically smooth flow ($0 < e^+ \leqslant 5$): In this range, the friction factor is the same for the rough and smooth pipes, because the projections of the roughness elements lie entirely within the laminar sublayer.
(2) Transitionally rough flow ($5 < e^+ \leqslant 70$): In this range, the projections of the roughness elements are of the same order of magnitude as the thickness of the laminar sublayer.
(3) Fully rough flow ($e^+ > 70$): The roughness function in this range is found to be independent of the roughness Reynolds number and it attains a constant value. The projections of the roughness elements extend beyond the laminar sublayer.

Nikuradse reported a constant value of 8.48 for the roughness function R for the fully rough region. However a number of investigators [3–8, 16–18] while investigating the behaviour of wire and rib roughnesses in tubes and ducts (both square and rectangular) have reported different values of the roughness function for fully rough flow. Further they have shown that the criterion of hydraulically smooth or fully rough and transitional flow regimes and the values of the roughness function depend not only on the roughness Reynolds number but also on the parameters describing the roughness and the flow. Han and Park [3] and Han et al. [5] and Liou and Hwang [16, 22] have also shown the dependence of this function on the channel aspect ratio.

In the investigation of sand grain roughness in tubes, Nikuradse has found that the roughness function R is a function of roughness Reynolds number e^+ alone. However, for other geometries of roughness elements and rectangular duct, roughness function R is not only a function of the roughness Reynolds number e^+ but also of the roughness geometrical parameters and duct aspect ratio. Hence, in general, the roughness function R is stated for a rectangular duct in the form

$$R = R(e/D_h, p/e, \alpha, e^+, W/H, \text{and rib shape}). \quad (3)$$

Dipprey and Sabersky [9] hypothesized that the law of wall similarity which has been shown by Nikuradse [2] to be valid for the velocity profile in roughened tubes, also applies to the temperature profile. They developed a heat transfer similarity law for flow in sand grain roughened tubes. They correlated turbulent heat transfer data for fluids of various Prandtl numbers and tubes of three different sand grain roughnesses using a heat transfer function, g (termed as g-function by them).

For the fully rough flow ($e^+ > 70$), Dipprey and Sabersky found that the heat transfer function was a function of only two variables: roughness Reynolds number and Prandtl number.

Webb et al. [7] used the law of wall similarity employed by Nikuradse and heat transfer–momentum transfer analogy extended by Dipprey and Sabersky, to correlate data for tubes with transverse repeated rib-roughness ($p/e = 10$–40). This general strategy has been successfully used to correlate friction and heat transfer results for different types of roughness elements by a large number of researchers [3–7, 10, 17–21]. Dependence of the g-function has also been shown on the roughness parameters. For a single fluid experiment, the Prandtl number is practically constant and hence the g-function can be stated in the general form as

$$g = g(e/D_h, p/e, \alpha, e^+, W/H, \text{and the rib shape}) \quad (4)$$

where

$$g = \{(f/2St) - 1\}\sqrt{2/f} + R. \quad (5)$$

However, many of the above mentioned investigators report negligible influence of one or other parameters on the heat transfer function.

Bergles [23] in his review paper states that in spite of difficulty in interpretation of these functions, this analogy based approach has emerged as a powerful tool for correlating the rough surface results.

3. Experimental program

A schematic of the experimental setup is shown in Fig. 2. The test facility consists of a rectangular duct set on the suction side of a 3.73 kW centrifugal blower. The duct cross-section was varied by changing the duct height, H from 12.5–30 mm (while the width of the duct was 150 mm) to give different channel aspect ratios. The lower and the two side wooden walls of the entire length of the duct have smooth surface. An unheated entrance duct length of 360 mm ($L/D_h = 7$–14.4, depending upon the duct depth) is provided. A short entrance length was chosen because for a roughened duct the thermally fully developed flow establishes in a short length of 2–3 hydraulic diameters [3, 22]. However, in the smooth rectangular ducts with thermal asymmetries larger development lengths are required compared to ducts with symmetrical heating [28]. The entrance length provided here is shown later to be sufficient. A 200 mm long exit section is installed to reduce any downstream effect on the test section. For the turbulent flow regime, ASHRAE standard 93-77 [24] recommends entry and exit lengths of

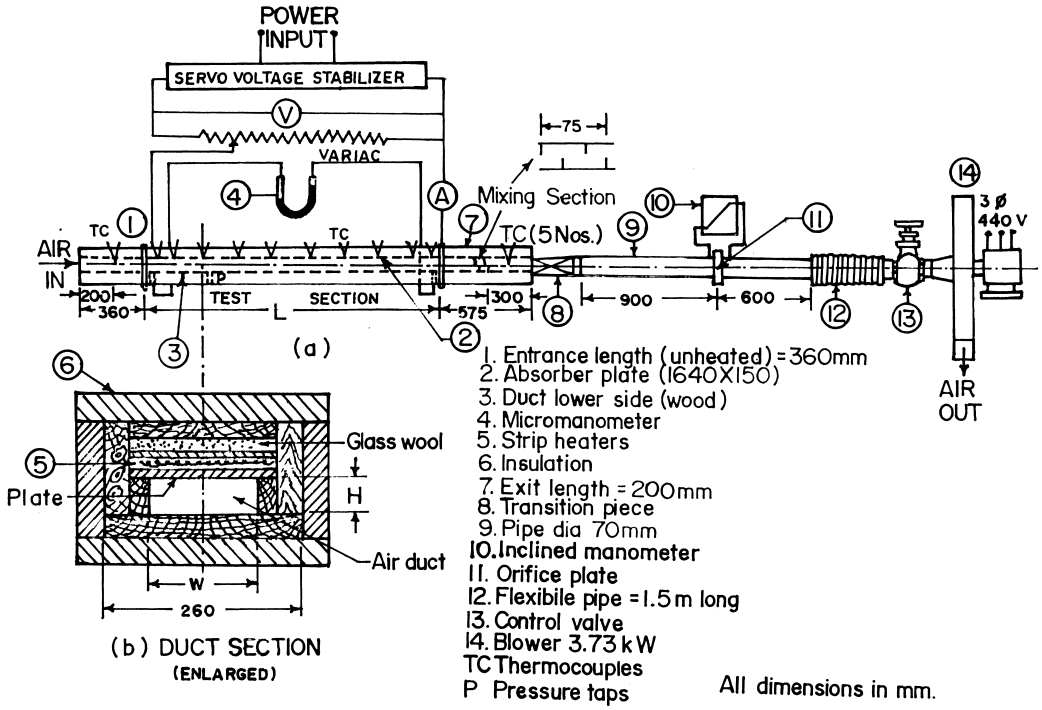

Fig. 2. Experimental setup.

$5\sqrt{WH}$ and $2.5\sqrt{WH}$, respectively, i.e. 340 mm and 170 mm, respectively, for the maximum duct depth employed in this case.

The test section length is 1.65 m resulting in length to hydraulic diameter ratios of 32–66 depending upon the duct height. Topside of the heated test section carried 6 mm thick aluminium plate with integral rib-roughness on the lower side. The topsides of the entry and exit lengths of the duct are covered with smooth face 8 mm thick plywood.

The electric heater assembly, as used by [1], consists of nine Nichrome strip heaters pressed against a 2 mm thick aluminium base plate. The heaters are connected in series and parallel to give combined maximum rating of 1 kW. AC stabilized power supply to the heaters has been provided through a variable transformer so that the heat flux to the absorber plate can be varied as desired. The space between the base plate of the heaters and the absorber plate was sealed. Thus the heat is transferred from the heater assembly to the absorber plate through radiation and conduction. The lower side of the heater assembly and upper side of the absorber plate are painted black to facilitate the transfer of heat. A 4 mm thick asbestos sheet followed by 10 mm thick layer of glass wool and 8 mm thick wood insulates the top of the heater's assembly. The outside of the entire setup, from test section inlet to the orifice plate, is insulated with 50 mm thick foamed polystyrene.

After passing through the heated test section, the air passes through the insulated mixing section. At the exit of the mixing chamber, uniform temperature of air was obtained (a temperature traverse at the exit of the mixing section confirmed negligible temperature variation). Five thermocouples arranged span-wise measure the exit air temperature after the mixing section. The exit end of the duct is connected, through a transitional section, to a 70 mm diameter pipe provided with a calibrated orifice plate. A 38 mm orifice plate with inclined tube manometer is used to measure the air flow rate.

Butt-welded 0.36 mm copper–constantan thermocouples, calibrated against mercury thermometer of 0.1°C least count, have been used for the temperature measurement. Ten thermocouples were provided along the axial centre line of the absorber plate in 5 mm diameter holes drilled 3–4 mm deep into the back of the plate while eight thermocouples at other locations were used to measure the span wise variation of absorber plate temperature.

It may be noted that due to the rib-roughness, a periodic variation of the plate surface temperature has been reported [3]. It has been thought that a small distance away from the ribbed surface, the equalization of the

temperature must take place. The thermocouple bead, thus, placed at a distance of about 2 mm from the roughened surface must be giving the average temperature. The difference in the surface temperature of the plate-ribbed side and the temperature at the thermocouple bead has been calculated to be negligible from the Fourier's conduction equation. For the maximum heat transfer rate of about 1200 W m^{-2} to the air, in the present investigation, thermal conductivity of 204 W m^{-1} K^{-1} of the aluminium absorber plate and depth of 2 mm, the difference between the two temperatures works out to be of the order of 0.01°C only.

The temperature of the base plate of the heater assembly was measured with seven thermocouples to estimate the transfer of heat to the absorber plate.

The thermocouple output was fed to a DC microvoltmeter through a selector switch.

Three pressure taps, located along the axial centre line of the smooth lower wall of the test section were used to measure the static pressure drops. A null balance type micromanometer having a least count of 0.01 mm of methyl alcohol is connected to the pressure taps.

Electric power to the heaters was measured by measuring current and voltage of the electric supply.

The integral rib-roughened absorber plates of aluminium were prepared by machining. The plates were made in two or three pieces and transverse grooves were machined on the plain side (opposite of the rib side) of the plates to reduce the effect of axial conduction of heat.

Table 2 gives the details of the roughness and other relevant system parameters. The minimum roughness height was chosen such that the laminar sublayer would be of the same order as roughness height at the lower flow Reynolds number. The maximum rib height was 1.68 mm so that the fin and flow passage blockage effects are negligible.

Each quoted rib height in Table 2 is the mean of three measurements taken along rib-length at each of 10 equally spaced axial stations along the test length. Each quoted rib pitch is the mean value determined from a count of complete pitches over an accurately measured distance of about 300 mm. The variation in the height along any one rib and between ribs was negligibly small, the maximum difference being 0.02 mm on a mean height of 0.75–1.68 mm. It may be pointed out that difficulties have been faced in getting plates manufactured of exact desired dimensions. Actual dimensions which are slightly different from the designed ones have been mentioned and used in the calculations, for example relative roughness pitch was to be 4.5, but the actual ones obtained are 4.58–4.87 (as seen in Table 2).

4. Experimental procedure

In order to reduce the effect of inaccuracy in the measurement of temperature, which strongly affects the accuracy of the calculation of the heat transfer coefficient, the temperature rise of the air through the duct was maintained greater than 10°C and the temperature difference between the heated plate and the bulk air temperature was kept above 20°C.

All readings were noted under steady state condition, which was assumed to have been obtained when the plate and the air outlet temperatures did not deviate over a 10 min period. The steady state for each run was observed to arrive in about 1.5–2 h.

5. Data reduction

The friction factor was determined from the measured values of pressure drop, δp, across the test length, $L_{f,}$ of 1.2 m (between the two points at 400 and 1600 mm from the inlet) and the mass flow rate, m, using the equation:

$$f = \frac{2(\delta p)\rho D_h}{4L_f G^2} \tag{6}$$

where $G = m/(WH)$ is the mass velocity of air, and $D_h = (4WH)/\{2(W+H)\}$ is the hydraulic diameter.

The heat transfer coefficient for the heated test section was calculated from:

$$h = \frac{Qu}{A_s(T_{pm} - T_{fm})} \tag{7}$$

where the heat transfer rate, Qu, to the air is given by

$$Qu = mC_p(T_o - T_i). \tag{8}$$

A_s is the heat transfer area, assumed to be the corresponding smooth plate area. The electric heating gives a condition of constant heat-flux boundary condition and the plate temperature varies in the direction of the air flow. In all the calculations, a mean plate temperature designated as T_{pm} has been used, which is calculated as integrated mean value of the plate temperature variation obtained experimentally. T_{fm} is the average fluid temperature.

The heat transfer coefficient has been used to determine the Nusselt number and Stanton number.

The thermophysical properties of air employed in the calculation of heat transfer and friction parameters, were picked up from available tables [27] corresponding to average fluid temperature T_{fm}. Further, the effect of humidity has been neglected since the relative humidity values during the experimentation were found to be low and variation was small, ranging between 20–35%.

From the analysis of the uncertainties in the measurements by various instruments [25], the uncertainties in the calculated values of various parameters are given below.

Reynolds number = ±2.12% (odds of 20:1)
Friction factor = ±4.56% (odds of 20 : 1)
Nusselt number = ±4.65% (odds of 20 : 1)

Table 2
Dimensions of roughened plates and test duct

Plate No.	Rib		Pitch	Chamfer	Duct		p/e	e/D_h	W/H
	Height e (mm)	Width w (mm)	p (mm)	angle ϕ (°)	Width W (mm)	Height H (mm)			
Angle of attack, $\alpha = 90°$									
1	1.68	1.77	7.69	0	148.8	30.9	4.58	0.0328	4.82
2	1.65	1.77	7.69	5	148.8	30.9	4.67	0.0322	4.82
3	1.58	1.77	7.69	10	148.8	30.9	4.87	0.0309	4.82
4	1.68	1.65	7.69	15	148.8	31.7	4.58	0.0321	4.69
5	1.68	1.65	7.69	−15	148.8	32.0	4.58	0.0319	4.65
6	1.44	1.77	7.69	14.5	148.8	30.9	5.41	0.0278	4.82
7	1.40	1.77	7.69	18	148.8	30.9	5.49	0.0274	4.82
8	1.07	1.77	7.69	18	148.8	30.9	7.19	0.0209	4.82
9	1.12	1.77	7.69	15	148.8	30.9	6.87	0.0219	4.82
10	0.75	1.10	5.25	0	148.8	30.9	7.00	0.0147	4.82
11	0.90	1.65	7.69	15	148.8	30.9	8.54	0.0176	4.82
12	0.90	1.65	7.69	15	148.8	19.2	8.54	0.0265	7.75
13	0.72	1.10	5.25	10	148.8	30.9	7.20	0.0141	4.82
14	0.72	1.10	5.25	10	148.8	19.2	7.29	0.0212	7.75
15	0.74	1.10	5.25	15	148.8	19.2	7.09	0.0218	7.75
16	0.74	1.10	5.25	15	148.8	12.4	7.09	0.0323	12.0
17	0.74	1.10	5.25	15	148.8	31.2	7.09	0.0143	4.77
18	0.74	1.10	5.25	15	148.8	24.4	7.09	0.0177	6.10
19	0.74	1.10	5.25	−15	148.8	30.9	7.09	0.0145	4.82
20	0.74	1.10	5.25	15	148.8	15.4	7.09	0.0265	9.66

Stanton number = ±5.01% (odds of 20 : 1)
Roughness function = ±3.33% (odds of 20 : 1)
Heat transfer function = ±8.61% (odds of 20 : 1)

where the Stanton number has been considered as a dependent dimensionless group ($St = Nu/Re\,Pr$) to arrive at the uncertainty.

6. Validity test and experimental results for smooth duct

Experimentation on roughened plates was preceded by data collection on smooth rectangular ducts. The smooth duct results have been presented in Fig. 3(a) and (b) along with the available results from the literature [26, 27]. The friction factor for a smooth rectangular duct is given by Bhatti and Shah [27] as

$$f = (1.0875 - 0.1125H/W) f_c \quad (9)$$

where f_c = friction factor for the circular duct = $0.0054 + 2.3\times10^{-8}\,Re^{1.5}$ for $2300 < Re < 4000 = 1.28\times10^{-3} + 0.1143\,Re^{-0.311}$ for $4000 < Re < 10^7$ and the Blasius relation, for $4000 \leqslant Re \leqslant 10^5$, is

$$f_c = 0.0791 Re^{-0.25}. \quad (10)$$

The Nussel number correlations of Gnielinski [26] and Dittus and Boetler [27] are given by equations (11) and (12), respectively,

$$Nu = 0.0214(Re^{0.8} - 100)\{1 + (D_h/L)^{0.66}\}(T_{fm}/T_{pm})^{0.45} Pr^{0.4} \quad for\ 2300 < Re < 10^6 \quad (11)$$

$$Nu = 0.024 Re^{0.8}\, Pr^{0.4}, \quad \text{for heating of fluid} \quad for\ 10^4 \leqslant Re \leqslant 1.24\times10^5. \quad (12)$$

The standard deviations of the present experimental friction data are ±5.9% and ±5.5% for the duct aspect ratios of 4.82 and 7.96, respectively, from the values predicted by equation (9) for $W/H = 4.82$ and equation (10). The maximum deviation of Nusselt number data is 6% from the values predicted by equations (11) and (12). Thus the good agreement between the values predicted, from equations (9)–(12), and the experimental values of the friction factor and Nusselt number ensures the accuracy of the experimental data collected with the present setup.

7. Results and discussion

Figure 4 shows the typical variations of plate and air temperatures along the length of the roughened test duct.

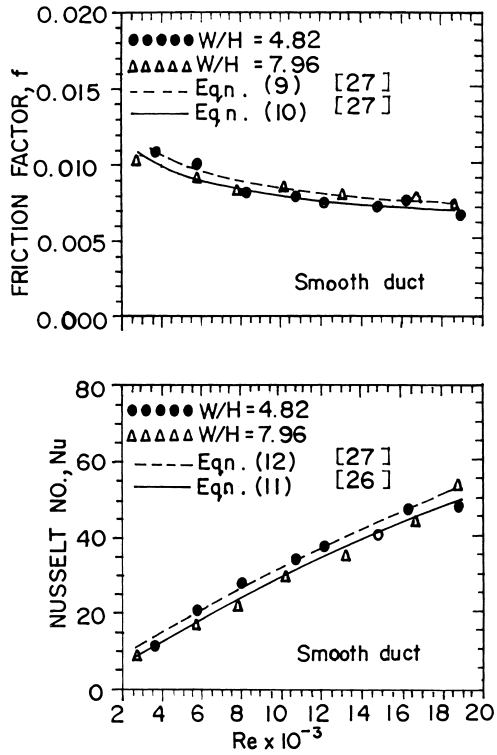

Fig. 3. Test results for smooth ducts: (a) friction factor vs. Reynolds number; (b) Nusselt number vs. Reynolds number.

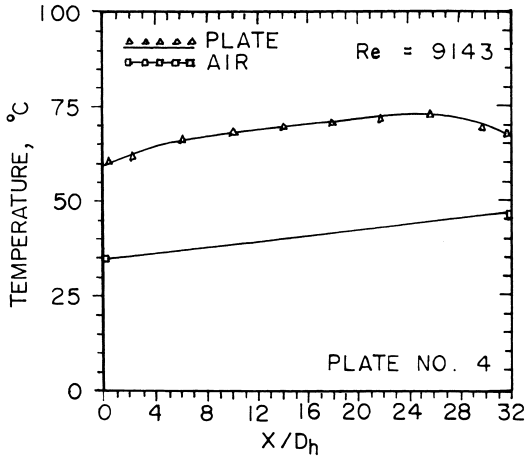

Fig. 4. Plate and air temperature distributions along the length of the test duct.

The longitudinal distribution of the air temperature has been represented as a straight line connecting the measured mean values at the inlet and exit of the duct. This assumption for the axial variation of air temperature is in line with Sparrow et al. [28], Novotny et al. [29] and Han [19]. For all the plates, the span wise plate temperature has been found to have the same value within $\pm 0.5^{\circ}$C. After a downstream distance, ranging from 6–8 hydraulic diameters in the heated section, as shown in Fig. 4, the plate temperature data paralleled the aforementioned bulk–air temperature straight line. This indicates establishment of the thermally fully developed flow after 6–8 hydraulic diameters. Thus the entrance region is quite short (20 and 10% of the flow length for the maximum and minimum duct depths, respectively) and the entrance length provided in the present experimental setup is sufficient. It can be seen that the average value of $(T_p - T_f)$ in the developing region is lower by less than 3°C against average value of this temperature difference of the order of 30°C. Thus, the higher heat transfer coefficient in the developing region will be within 10% of the average value. The overall effect on the heat transfer coefficient for the whole heat transfer area is, thus, of the order of 1–2% only. The drop in the plate temperature near the end section appears to be due to the end effect. The temperature of the wall decreased near the ends because in these regions, the wall does not see as much of the heated wall and hence receives less radiative energy than the part of the wall in the centre of the duct. This effect observed here is similar to that observed and reported by Tan and Charters [30] and Gupta [31]. The mean plate temperature has been calculated by integration of the equation of the best fit curve through the plate temperature data points along the plate length.

The effect of various flow and roughness parameters on heat transfer and friction characteristics for flow of air in rectangular ducts of different aspect ratios of the present investigation are being discussed below. Results have also been compared with those of the smooth duct under similar flow and thermal boundary conditions to demonstrate enhancement in the heat transfer coefficient and friction factor.

7.1. Variation of the Stanton number and friction factor with the Reynolds number

Figures 5(a) and (b) show the variation of Stanton number with Reynolds number for the transverse ribs having nearly fixed values of relative roughness pitch of 4.5 and 7.0, respectively, but the chamfer angle varying between -15–15°. It can be seen from these figures that the Stanton number values increase with the Reynolds number and attain some maximum values. In Fig. 5(a), the Stanton number after attaining the maximum values at Reynolds number of about 8000 drop slightly and the curves become nearly parallel to the curve of the smooth surface except for the surface with -15° chamfer. But in Fig. 5(b) because of the lower roughness height of 0.014, the Stanton number is seen to attain its maximum value at higher Reynolds number. Thus, the Stanton number depends on both the Reynolds number and the relative

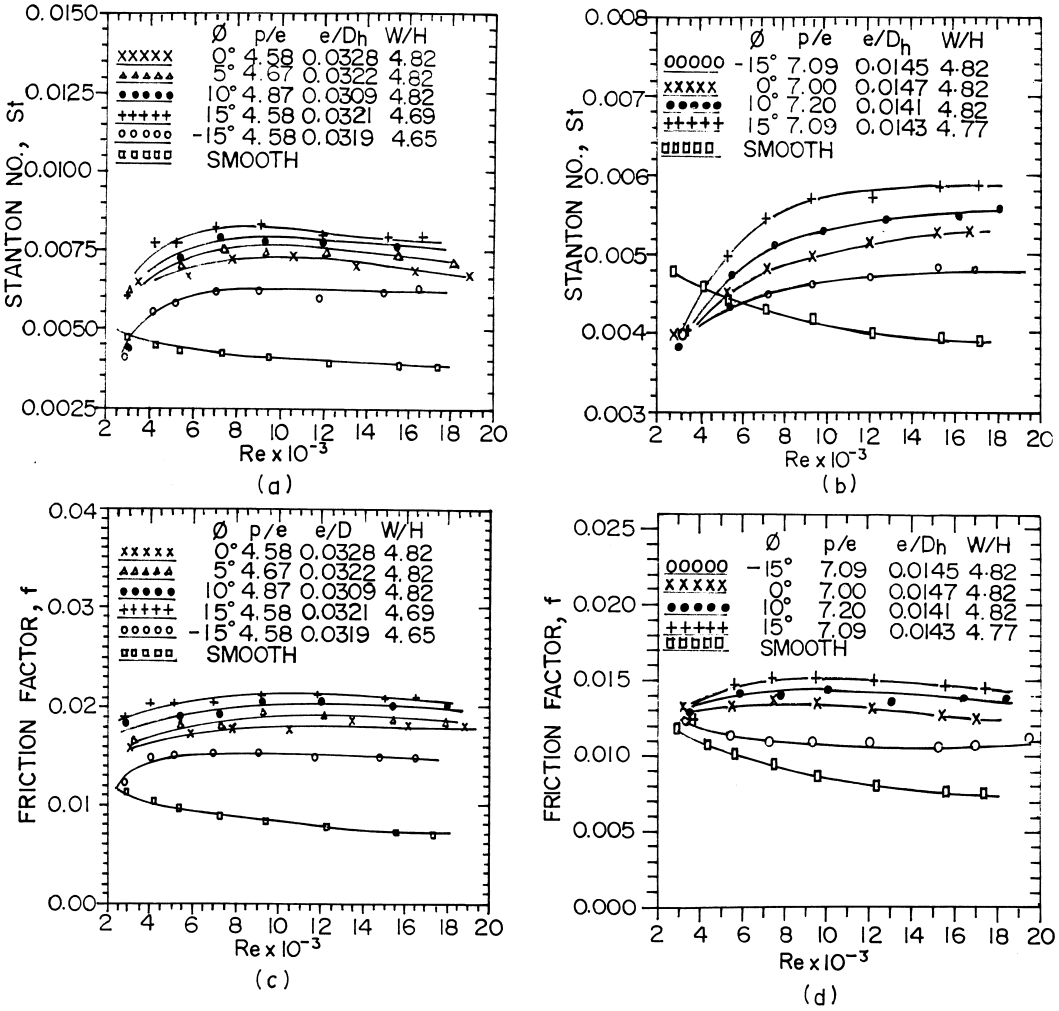

Fig. 5. (a) Variation of the Stanton number with the Reynolds number ($p/e = 4.5$). (b) Variation of the Stanton number with the Reynolds number ($p/e = 7$). (c) Variation of the friction factor with the Reynolds number ($p/e = 4.5$). (d) Variation of the friction factor with the Reynolds number ($p/e = 7$).

roughness height. The combined effect of the Reynolds number and the relative roughness height is further discussed later on.

It is seen in Figs 5(a) and (b) that at low flow rates, the value of the Stanton number for the rough surface is lower than that for a smooth surface. It is attributed to the fact that at the low flow rates the flow is still in the hydraulically smooth regime and the laminar sublayer thickness increases as the flow is retarded by the roughness elements. When the rib relative roughness height is greater as in Fig. 5(a), compared to that in Fig. 5(b), the roughness elements start projecting earlier beyond the laminar sublayer as the Reynolds number increases.

Figure 5(c) shows the plots of experimental values of the friction factor as a function of the Reynolds number for surface with transverse ribs at nearly fixed values of relative roughness pitch of 4.6. The friction factor is found to be independent of the Reynolds number at high flow rates ($Re > 6000$). Similar behaviour of the variation of the friction factor with the Reynolds number can also been seen from Fig. 5(d) for the surface with transverse ribs at relative roughness pitch of 7.0.

The variation of the Stanton number and the friction factor with the Reynolds number is now explained. At low Reynolds numbers, the roughened surface Stanton number and friction factor values are nearly those of the smooth surfaces because the roughness elements lie within the laminar sublayer and the laminar sublayer is the major component of the heat transfer resistance. As the Reynolds number increases, the roughness elements

begin to project beyond the laminar sublayer because the boundary layer thickness decreases with an increase in the Reynolds number. This reduction in the boundary layer thickness increases the heat transfer rate. In addition to this, there is local contribution to the heat removal by the vortices originating from the roughness elements. The shedding of vortices also causes additional loss of energy resulting in increased friction factor. Thus, the Stanton number and friction factor curves deviate from the smooth duct turbulent Stanton number and friction factor curves. When the Reynolds number further increases, the roughness elements project deeper into the turbulent region. Finally, with the increase in the Reynolds number, the thickness of laminar sublayer becomes very small and the energy loss due to vortices now attains a constant value and is independent of viscous effect [34]. The heat removal from the surface also attains its maximum value. Further increase in the Reynolds number no longer increases the friction factor. The beginning of the independence of the friction factor on the Reynolds number is classified as the fully rough region and the Reynolds number corresponding to the start of region of independence of the friction factor is termed as the critical Reynolds number, Re_c [35]. In the case of fully rough flow conditions ($Re > Re_c$), the roughened surface behaves like a normal surface with an enhanced value of friction factor (becoming constant in the fully rough region, as mentioned above), but the Stanton number gradually starts falling and the curve becomes nearly parallel to the smooth surface curve. In the fully rough region, the form drag overrides the skin friction and hence the friction factor becomes constant, independent of the Reynolds number. However, there is no counterpart of form drag that would contribute to the Stanton number, and hence Stanton number vs. Reynolds number curve continues to behave like a smooth surface. Sheriff and Gumley [35] and Vilemas and Simonis [36] have observed that the Stanton number shows first an increase and then a decrease with an increase in the Reynolds number for flow through annuli with outer surface of the inner tube (core) roughened. The roughness on the inner core was obtained by Sheriff and Gumley [35] by wrapping circular wire on the inner core; and by Vilemas and Simonis [36] by providing rectangular ribs on the inner core. For higher relative roughness heights and at high Reynolds numbers, they found that the Stanton number curve became parallel to the smooth surface curve. Burgoyne et al. [37] observed, for flow in annuli with transverse ribs on inner tube, that the variation of the Stanton number with the Reynolds number depends also on relative roughness height. They found that, while for the higher roughness heights the Stanton number curves became parallel to the smooth surface, the Stanton number increases slightly for the surfaces with very small relative roughness heights.

It was observed in Figs 5(a) and (b) that the difference between the roughened and the smooth duct Stanton numbers varies with the Reynolds number. Thus, it is interesting to see the effect of roughness on the Stanton number and friction factor enhancement relative to the smooth duct. Figures 6(a) and (b) are the plots of Stanton number ratio, St/St_s, and friction factor ratio, f/f_s, respectively. Both the Stanton number and friction factor ratios are seen to increase with an increase in the chamfer angle from -15 to 15°. The Stanton number ratio increases at high rates up to Reynolds number of about 8000 and then increases marginally (3–8%). The variation of the Stanton number with the Reynolds number

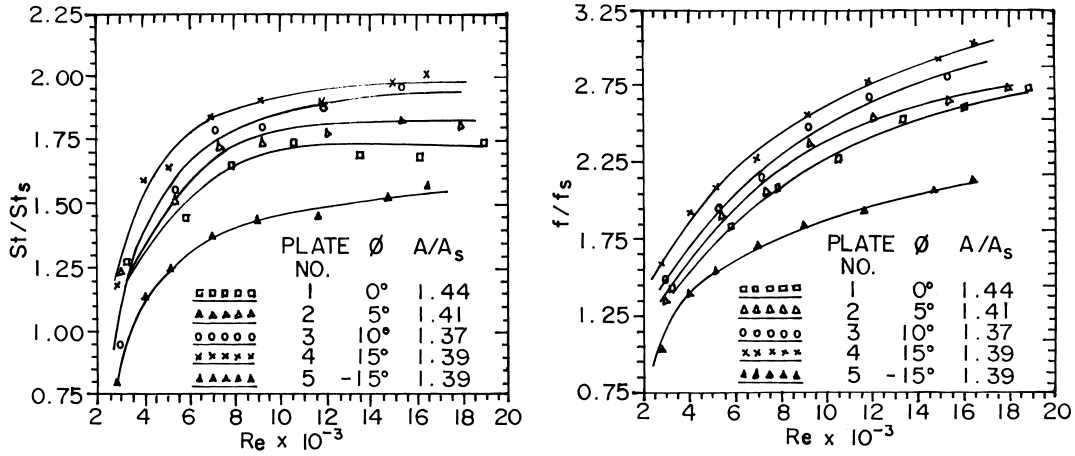

Fig. 6. (a) Stanton number ratio vs. the Reynolds number as function of the chamfer angle. (b) Friction factor ratio vs. the Reynolds number as function of the chamfer angle.

for the roughened surface with respect to the smooth surface behaviour has been discussed above and hence this variation of Stanton number ratio is expected.

It can be seen that for lower values of the Reynolds number, the improvement over the smooth duct Stanton number is small. At very low Reynolds numbers (<4000), it can be seen from Fig. 6(a) that the value of Stanton number ratio St/St_s is unity or even less than unity (less than unity means that the performance of smooth surface is better). The value of less than unity at very low flow rates may be attributed to the fact that the laminar sublayer thickness increases as the flow is retarded by roughness elements. The observation is similar to that observed by Gupta [31], Ligrani et al. [38] and Pedisius and Slanciauskas [39].

7.2. Effect of the chamfer angle

Figures 5(a) and (b) show that the Stanton number values increase with increase in chamfer angle from -15 to 15°. It can be seen from Fig. 5(c) that the friction factor values increase with an increase in the chamfer angle from -15 to 15°. The strong effect of chamfering on the friction factor can also be seen from Fig. 5(d) for the surface with transverse ribs at relative roughness pitch of 7.0.

Figure 7 is a typical plot of the Stanton number and friction factor vs. the chamfer angle for the relative roughness pitch p/e of 4.5 surface at the Reynolds number of 10 000. The Stanton number and friction factor increase by 16 and 18%, respectively, for an increase in the chamfer angle from 0 to 15°. The rates of change in the Stanton number and friction factor decrease with an increase in the chamfer angle. It can be seen from the

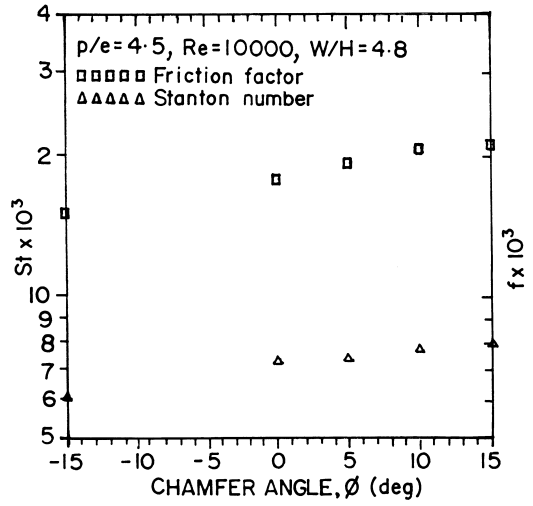

Fig. 7. Stanton number and friction factor vs. chamfer angle for $p/e = 4.5$ and $Re = 10\,000$.

results of 15 and 18° chamfered surfaces with relative roughness pitches of 5.5 and 7.0, plotted in Figs 8(a)–(d), that the friction factors for the two surfaces are almost the same for the entire range of flow Reynolds numbers. The Stanton numbers for 15 and 18° surfaces are found to be either equal (for $p/e \approx 7$ surface) or higher for the 15° surface (for $p/e \approx 5.5$ surface). The likely reason for this observation is that at around 15° chamfer angle the turbulence due to the shedding of vortices reaches its maximum and further increase in the chamfer angle does not increase the frequency of vortex shedding.

Thus, it is seen that with increase in the chamfer angle from -15 to 0 to 15°, the Stanton number increases. As no further increase in Stanton number is found for the change of chamfer angle from 15 to 18°, it can, therefore, be concluded that the Stanton number takes the maximum value at the chamfer angle of 15°.

Williams et al. [10] and Williams and Watts [11] have reported a strong effect of chamfering of rectangular ribs for the flow through circular annuli with ribs on the outer surface of the inner tube. Williams et al. [10] observed that the Stanton number for 13° chamfered surface was higher than the 0 and 22° chamfered surfaces by about 8 and 11%, respectively. The friction factor was found to be higher by about 10% for the 13° chamfer angle than the friction factor for the 0° chamfer. They observed only a slight decrease in the friction factor for an increase in the chamfer angle from 13 to 22°. They reported that the enhancements in the Stanton number and friction factor were seen to be higher for relative roughness pitch values of less than 7 (values or plots are not given in the paper). Thus, the trends in the Stanton number and friction factor variations for a rectangular duct with roughness and heat flux to one broad wall, in the present study, are in qualitative agreement with the results of Williams et al. [10], which are for the flow in the circular annuli.

Study of flow patterns by Williams and Watts [11] as depicted in Fig. 9 revealed that with the square section rib ($\phi = 0°$) at relative roughness pitch of 3, a standing vortex was formed between the ribs filling approximately two thirds of the cavity, and the energy interchange with the main flow was found to be only sufficient to provide vortex shedding occasionally. Thus the mean level of flow disturbance in the main flow above the ribs was small. But with the chamfered ribs ($\phi = 10°$), they observed that the vortex between the ribs was more vigorous, growing to full cavity size and shedding more frequently thus causing a much larger area of disturbance above the ribs. Thus the increase in the Stanton number and friction factor with the increase in the chamfer angle from 0 to 15° can be attributed to the more frequent shedding of vortices and hence causing greater heat removal from the surface as well as more frictional loss. The decrease in the Stanton number and friction factor values for the negative chamfer can be attributed to the suppression of

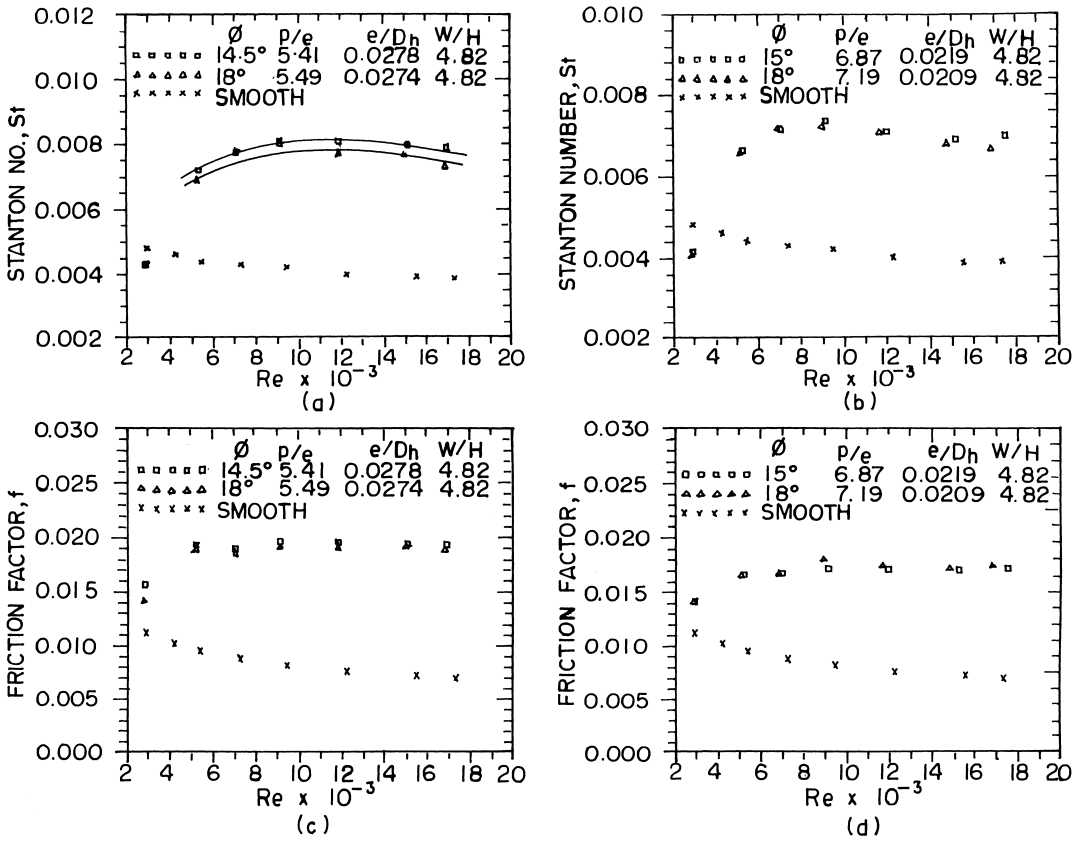

Fig. 8. (a) Effect of the chamfer angle ($\geqslant 14.5°$) on the Stanton number ($p/e = 5.5$). (b) Effect of the chamfer angle ($\geqslant 15°$) on the Stanton number ($p/e = 7$). (c) Effect of the chamfer angle ($\geqslant 14.5°$) on the friction factor ($p/e = 5.5$). (d) Effect of the chamfer angle ($\geqslant 15°$) on the friction factor ($p/e = 7$).

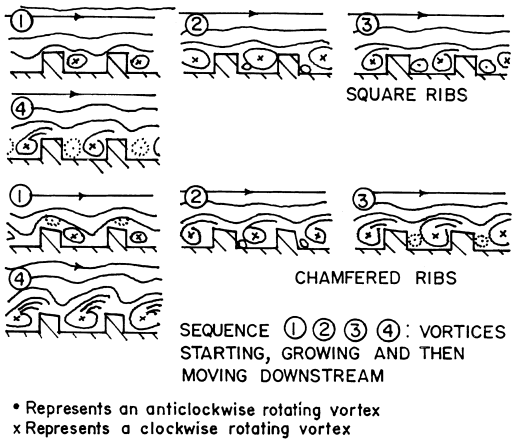

Fig. 9. Flow patterns reproduced from [11] for square ($\phi = 0°$) and chamfered ($\phi = 10°$) fibs; $p/e = 3$.

the shedding of vortices as the flow is likely to skim over the ribs.

Wilkie [13] has reported that a slight chamfer is sufficient to cause a reduction of 7.8% in the friction factor for the relative roughness pitch of 5.5 and of 5.8% for the relative roughness pitch of 13.3. In both instances, further chamfering has no effect. The values of the first angle and the angle after further chamfering are not clearly mentioned by Wilkie and probably are 22.5 and 45°, respectively. He has further reported that the friction factor has been found to be 8% higher with the sharp corner facing upstream ($+\text{ve}\phi$) than when facing downstream ($-\text{ve}\phi$). He observed a significant difference in axial pressure gradients before and after chamfering. The effect of chamfering was also confirmed by Schlieren studies.

It may be pointed out that the substantial enhancement in the Stanton number observed as a result of providing rib roughness elements is due to the generation of additional turbulence and not just due to an accompanying increase in heat transfer area, although the calculation of heat transfer coefficient has been based on the assumed datum area of corresponding smooth surface. It can be seen from Fig. 6(a) that the increase in the ratio of Stan-

ton numbers (85% for $\phi = 15^\circ$ surface at $Re \approx 8000$) is much higher than the increase in area ratio A/A_s (39%) for the surface. From the figure, it can also be seen that for the rectangular rib ($\phi = 0^\circ$), the increase in the Stanton number ratio is 65% while the increase in the area ratio is 44%. Thus the increase of about 20% in the Stanton number for 15° chamfered surface over 0° chamfered surface can be attributed to the increased turbulence due to the chamfering of the rib head.

7.3. Effect of the relative roughness height

Figure 10(a), which is a plot of the Stanton number vs. the Reynolds number for the surfaces with nearly the same value of relative roughness pitch and with different relative roughness heights, shows that the Stanton number increases with an increase of the relative roughness height. For the lower value of the Reynolds number ($Re < 4000$) the value of the Stanton number for the roughened surface approaches that of the smooth surface. A similar effect of the relative roughness height on the friction factor can be seen in Fig. 10(b) which is a plot of the friction factor against the Reynolds number for different values of relative roughness heights.

From an observation of the Fig. 10(a), it can be seen that the maximum value of the Stanton number is a function of both the relative roughness height and the Reynolds number. Further the shorter ribs ($e/D_h = 0.0143$) show a gradual variation as compared to the taller ribs. The start of the fully rough region, as discussed earlier, has been shown [13] to depend both upon the relative roughness height and the Reynolds number and is clearly defined by the roughness Reynolds number. The roughness Reynolds number, defined by equation (2), combines the friction factor, relative roughness height and the flow Reynolds number. Nikuradse [2] has clearly established that the hydraulically smooth, transitionally and fully rough flow regimes are well defined by the roughness Reynolds number. Hence. 62 data points of Stanton number for eight roughened plates, comprising of relative roughness height from 0.0143 to 0.0328, chamfer angle from 0 to 15°, relative roughness pitch from 4.58 to 8.54, and duct aspect ratios of 4.77 and 7.75, have been plotted against roughness Reynolds number in Fig. 11. It can be seen that the maxima of the Stanton numbers for these plates with different flow and roughness geometries occur at roughness Reynolds number of about 20–25.

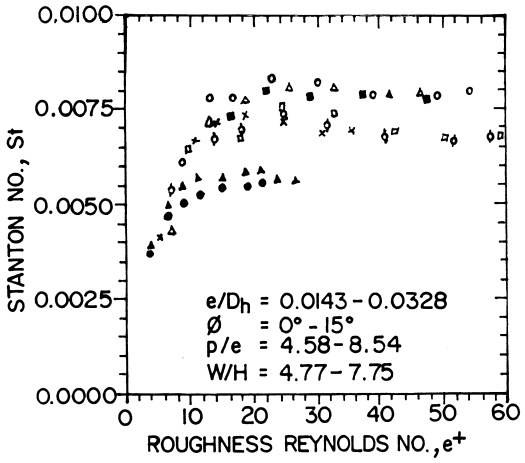

Fig. 11. Variation of the Stanton number with the roughness Reynolds number (□ Plate No. 1, ■ Plate No. 3, ○ Plate No. 4, △ Plate No. 6, × Plate No. 9, ○ Plate No. 12, ● Plate No. 13, ▲ Plate No. 17).

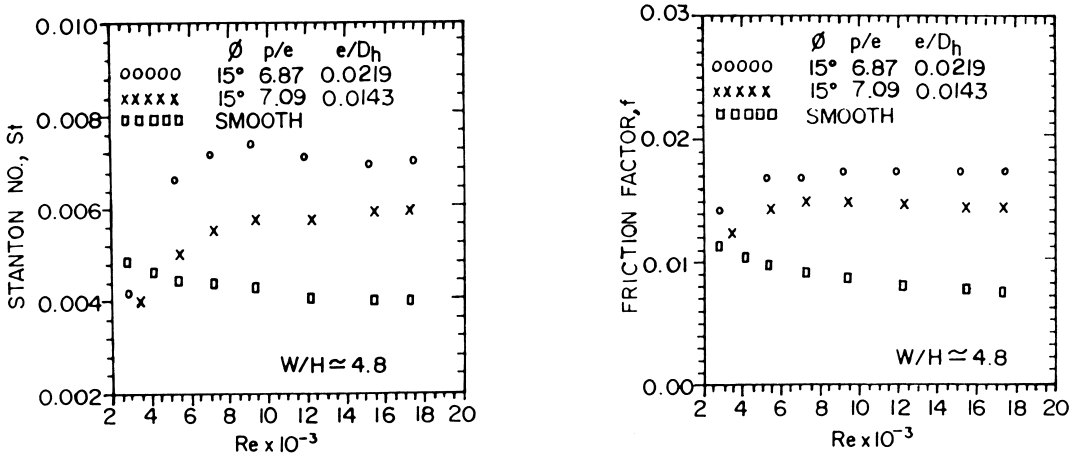

Fig. 10. (a) Effect of the relative roughness height on the Stanton number. (b) Effect of the relative roughness height on the friction factor.

It may be noted that Webb [32] also found that for the transverse rib roughness in tubes, the maximum value of the Stanton number was at roughness Reynolds number of 25. Gupta [31] has also reported occurrence of maxima in Stanton number at roughness Reynolds number of 25 for wire roughness on one broad wall of a rectangular cross-section duct.

7.4. Effect of the aspect ratio

Figures 12(a) and (b) show the effect of the aspect ratio, W/H, on Stanton number and friction factor ratios, respectively. The effect of the aspect ratio on the smooth duct heat transfer and friction characteristics has also been reported in the present investigation in Fig. 3(a) and (b). Hence, for a justifiable comparison, the Stanton number and friction factor ratios have been selected. It can be seen that while the Stanton number ratio St/St_s is decreased by about 5% with an increase in the aspect ratio from 4.82 to 7.75, the friction factor ratio f/f_s increased by about 20% for corresponding flow conditions. Thus, the lower aspect ratio duct provides a better heat transfer performance. Han and Park [3] investigated the effect of the channel aspect ratio on heat transfer and friction characteristics for the developing flow in short rectangular channels ($L/D_h = 10$–15) with opposite rib roughened walls. The channel aspect ratio was varied as 1, 2 and 4. At the flow Reynolds number of 30 000, the values of the Nusselt number ratio (Nu/Nu_s) for both rectangular channels ($W/H = 2$ and 4) have been reported to be almost the same, while the friction factor ratios (f/f_s) of 7 and 16 for these ducts. For equal pumping power, the heat transfer performance of a square channel has been shown to be slightly better than that of a rectangular duct with aspect ratio of 2 and about 10% better than that of the duct with aspect ratio of 4.

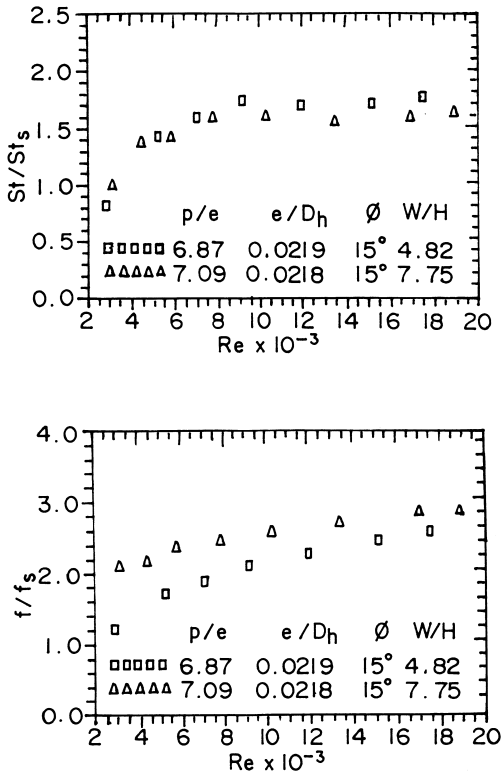

Fig. 12. (a) Effect of the aspect ratio on the Stanton number ratio. (b) Effect of the aspect ratio on the friction factor ratio.

Transient and turbulent flows in noncircular smooth ducts are accompanied by secondary flows [27]. This secondary flow is stronger in the case of roughened ducts. The region occupied by the secondary flow decreases with the increase in the aspect ratio. Further, in large aspect ratio ducts, the turbulence created at the roughened wall may increase friction at the opposite wall. These factors may be the likely reasons for the observed effect of increasing f with the aspect ratio. The smooth wall facing the heated roughened wall is adiabatic; hence, the increased turbulence at this wall (due to the roughness at the opposite heated wall) does not contribute to the increase in the Stanton number. Further, as the aspect ratio increases the relative effect of secondary flow on the Stanton number decreases. The combined effect of these factors results in the decrease in the Stanton number with the aspect ratio.

8. Development of correlations

For the results to be useful for the designers, general correlations are presented here which cover all combinations of the geometric and flow parameters within the range given in Table 1. The results of the present investigation have been correlated in terms of the roughness and heat transfer functions given by equations (1) and (5), respectively, with $E = 3.75$ in equation (1).

It has been shown by many investigators [2, 9, 18, 33] that the roughness function and the heat transfer function are independent of the relative roughness height. However, Lewis [40] has remarked that if the relative roughness height is not small, then both the roughness function and heat transfer function lose their local character; and some other analysis, which takes into account, for example, the acceleration of flow, must be considered. Figures 13(a) and (b) are the plots of the roughness function and heat transfer function, respectively, vs. the roughness Reynolds number for surfaces with different relative roughness heights and with nearly the same values of other roughness parameters and the duct aspect ratio. These plots of the present investigation show that the roughness and heat transfer functions are independent of relative roughness heights.

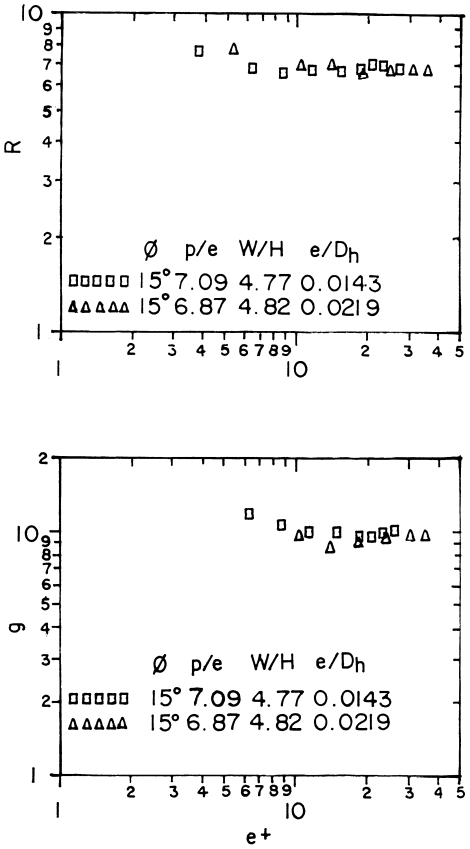

Fig. 13. (a) Effect of the relative roughness height on the roughness function. (b) Effect of the relative roughness height on the heat transfer function.

The basic equation of the heat transfer function g, equation (5), consists of the roughness function R, hence the correlation of roughness function R is presented first.

These correlations have been developed using the method of cross plotting adopted by Webb et al. [7] and Sethumadhavan and Rao [18]. The equations of the best fit curves have been determined using Grapher version 1.79D and a Personal Computer.

8.1. Friction correlation

The roughness function data when plotted against the chamfer angle were found to vary exponentially. Hence, the roughness function data have been plotted against the chamfer angle in Fig. 14(a) on a semi-log scale. The equation of the best-fit curve through the data points yields

$$\ln(R) = \ln C_1 - 0.0078\phi. \tag{13}$$

The above relation can be written as

$$R = C_1 e^{-0.0078\phi} \tag{14}$$

where C_1 is a function of other influencing parameters.

It has been shown that apart from the rib chamfer angle, the duct aspect ratio is a parameter having a significant effect on the friction factor. In order to bring out the effect of the duct aspect ratio in the friction correlation, the values of $(R/e^{-0.0078\phi})$ have been plotted against the duct aspect ratio (4.65–7.75) on a log–log scale in Fig. 14(b). The following equation of the best fit curve is obtained:

$$\frac{R}{e^{-0.0078\phi}} = C_2[W/H]^{-0.4} \tag{15}$$

where the constant of proportionality C_2 would be a function of the remaining parameters i.e. of the relative roughness pitch, p/e, and the roughness Reynolds number, e^+.

It can be seen from Fig. 14(c) that the variation in the value of the roughness function with change in the aspect ratio from 7.75–12 is very small and hence the relationship given by equation (15) can be used for the complete range of the present investigation with the condition that for $W/H > 7.75$, use $W/H = 7.75$.

Now to incorporate the effect of the relative roughness pitch, the values of $[R/\{e^{-0.0078\phi}(W/H)^{-0.4}\}]$ have been plotted against the relative roughness pitch in Fig. 14(d) on a log–log scale. The following relation fitted the data points closely:

$$\frac{R}{e^{-0.0078\phi}(W/H)^{-0.4}} = C_3(p/e)^{2.695}\exp\left[-0.762\{\ln(p/e)\}^2\right] \tag{16}$$

where C_3 is a function of the remaining parameter i.e. the roughness Reynolds number.

Finally, a plot of $R/[\{e^{-0.0078\phi}(W/H)^{-0.4}\}(p/e)^{2.695}\exp\{-0.762(\ln p/e)^2\}]$ vs. the roughness Reynolds number, as shown in Fig. 14(e), gives the final correlation as:

$$R = 1.66e^{-0.0078\phi}(W/H)^{-0.4}(p/e)^{2.695} \times \exp\left[-0.762\{\ln(p/e)\}^2\right](e^+)^{-0.075} \quad \text{for } 5 \leqslant e^+ < 20 \tag{17}$$

$$R = 1.325e^{-0.0078\phi}(W/H)^{-0.4}(p/e)^{2.695} \times \exp\left[-0.762\{\ln(p/e)\}^2\right] \quad \text{for } 20 \leqslant e^+ \leqslant 60 \tag{18}$$

for $W/H > 7.75$ use $W/H = 7.75$ in equations (17) and (18).

The values of the roughness function obtained from the proposed correlation have been compared with those obtained from experimental data in Fig. 14(f). 94% (140 out of 149) of the total data points are within $\pm 8\%$. The standard deviation is found to be $\pm 4.35\%$. Thus, the present correlation can predict the values of the rough-

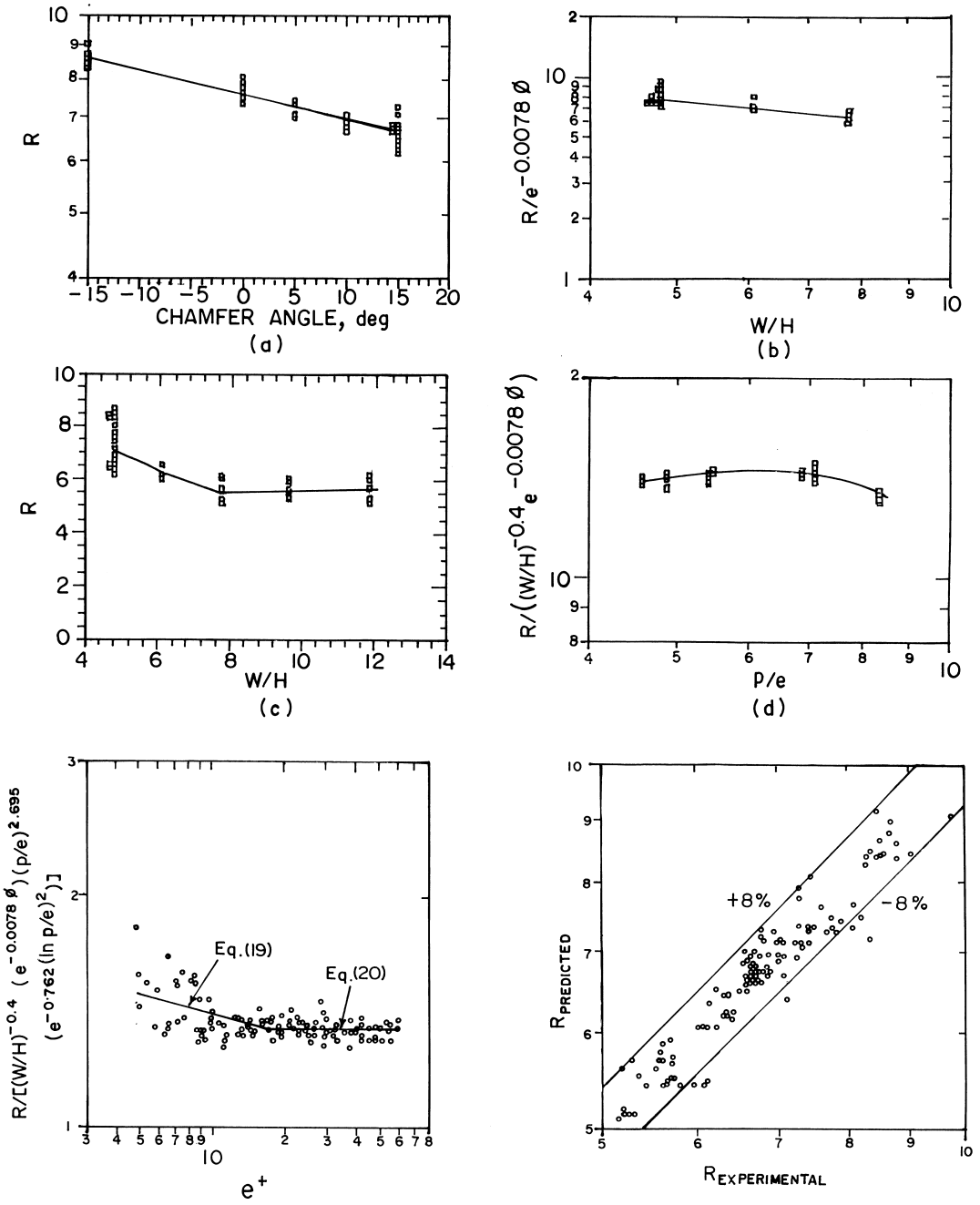

Fig. 14. (a) Effect of the chamfer angle on the roughness function (75 data points of 10 plates). (b) Effect of the aspect ratio on the roughness function: $W/H = 4.65$–7.75 (120 data points of 18 plates). (c) Effect of the aspect ratio on the roughness function; $W/H = 4.65$–12 (132 data points of 20 plates). (d) Effect of the relative roughness pitch on the roughness function (60 data points of 9 plates). (e) Final friction correlation. (f) Comparison of the experimental roughness function with the roughness function calculated from equations (17) and (18).

ness function quite satisfactorily in the range of parameters investigated.

It may be noted that the roughness function is independent of the roughness Reynolds number e^+ for the range when e^+ is greater than 20, as seen from Fig. 14(e). This indicates the initiation of the fully rough region at

about $e^+ = 20$ for the roughness of the present investigations. Although, the dependence of the roughness function on the roughness Reynolds number values of less than 20 can be clearly seen, the data could not be correlated very well due to a large scatter of experimental data.

Figure 14(d) shows that the roughness function first increases by about 5% with increase in the relative roughness pitch from about 4.5 to 7 and then decreases by about 10% for increase in relative roughness pitch from about 7 to 8.5. It may be noted that, in general, a lower value of the roughness function indicates a higher value of the friction factor. The value of relative roughness pitch of approximately 7.0 also corresponds to the minimum rib spacing necessary for the flow, which separates at the rib, to reattach. Thus, it appears that the enhancement for the chamfered closed space ribs ($p/e \leqslant 7$) is more due to the increased vortex shedding while in the case of widely spaced ribs, the flow reattachment contributes more to the enhancement. A detailed flow visualization study is needed to confirm the hypothesis presented here.

8.2. Heat transfer correlation

The mathematical procedure adopted for the development of the heat transfer correlation is the same as the one adopted for the friction correlation, hence the methodology is given only in brief.

The heat transfer function data are plotted in Fig. 15(a) against the chamfer angle on a semi-log scale. The equation of the best-fit curve yields

$$\ln(g) = \ln C_4 - 0.006\phi \tag{19}$$

or

$$g = C_4 e^{-0.006\phi} \tag{20}$$

where C_4 is a function of other influencing parameters.

Figure 15(b) shows a plot of the values of $(g/e^{-0.006\phi})$ against the duct aspect ratio (4.65–9.66) on a log–log scale. The equation of the best-fit curve gives

$$g = C_5 e^{-0.006\phi}(W/H)^{0.5} \tag{21}$$

where C_5 is a function of the remaining two parameters i.e. the relative roughness pitch and the roughness Reynolds number.

It can be seen in Fig. 15(c) that the correlation can be extended to the duct aspect ratio of 12 with the condition that for $W/H > 10$ use $W/H = 10$.

The plot of function $[g/\{e^{-0.006\phi}(W/H)^{0.5}\}]$ vs. the relative roughness pitch is shown in Fig. 15(d) on a log–log scale. The equation of the best-fit curve is

$$\frac{g}{e^{-0.006\phi}(W/H)^{0.5}} = C_6(p/e)^{-2.56} \times \exp\left[0.7343\{\ln(p/e)\}^2\right] \tag{22}$$

where C_6 is a function of the remaining parameter, i.e. the roughness Reynolds number.

Finally a plot of $g/[e^{-0.006\phi}(W/H)^{0.5}(p/e)^{-2.56} \exp\{0.7343(\ln p/e)^2\}]$ vs. the roughness Reynolds number, as shown in Fig. 15(e), gives the final correlation as

$$g = 103.77e^{-0.006\phi}(W/H)^{0.5}(p/e)^{-2.56} \times \exp\left[0.7343\{\ln(p/e)\}^2\right](e^+)^{-0.31} \quad \text{for } 7 \leqslant e^+ < 20 \tag{23}$$

$$g = 32.26e^{-0.006\phi}(W/H)^{0.5}(p/e)^{-2.56} \times \exp\left[0.7343\{\ln(p/e)\}^2\right](e^+)^{0.08} \quad \text{for } 20 \leqslant e^+ \leqslant 60 \tag{24}$$

when $W/H > 10$ use $W/H = 10$ in equations (23) and (24).

The values of the heat transfer function, for the roughness Reynolds number greater than 10, obtained from the proposed correlation have been compared with those obtained from experimental data in Fig. 15(f). Eighty-eight per cent of the data points lie within $\pm 10\%$ (106 out of 120). The standard deviation is $\pm 6.3\%$. Thus, the present heat transfer correlation can predict the values of the heat transfer function quite satisfactorily in the range of parameters investigated in the present work. The higher scatter than the friction correlation can be attributed to the higher uncertainty of $\pm 8.61\%$ in the heat transfer function compared to $\pm 3.33\%$ for the roughness function as reported earlier.

It can be seen in Fig. 15(e) that the minimum of the plot lies at roughness Reynolds number of about 20. In general, a low value of the heat transfer function indicates a high value of the Stanton number. Occurrence of maxima in the Stanton number at roughness Reynolds number of about 20–25 has been observed in Fig. 11 and discussed thereupon.

Very scarce data are available for the transitional flow in rectangular ducts with rib-roughness on one broad wall subjected to uniform heat flux. In the transition regime, each roughness has its own characteristic behaviour [41] and the value of the roughness function and heat transfer function must be different for different types of roughnesses.

Different investigators report different degrees of dependence of the roughness and heat transfer functions on roughness parameters for flow in roughened tubes or rectangular ducts with two or all the four walls roughened and subject to uniform heat flux.

Webb et al. [7] and Han et al. [4] have reported that the roughness function is not a function of the roughness Reynolds number for values of the roughness Reynolds number greater than 25–35. In the present study, this value is found to be about 20.

Dalle Donne and Meyer [17] conducted experimental investigation for flow of air in circular annuli with rough-

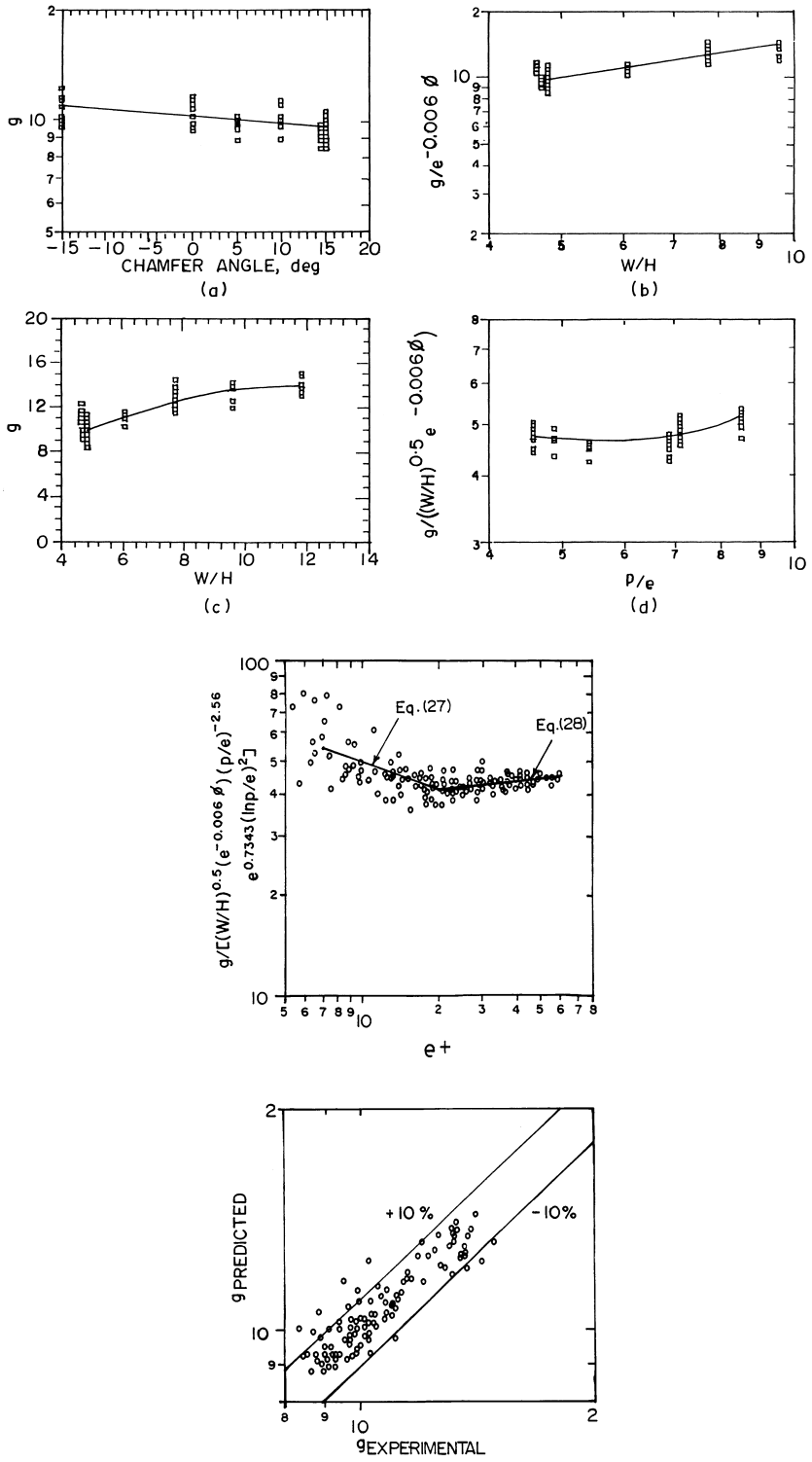

Fig. 15. (a) Effect of the chamfer angle on the heat transfer function (75 data points of 10 plates). (b) Effect of the aspect ratio on the heat transfer function; $W/H = 4.65$–9.66 (108 data points of 18 plates). (c) Effect of the aspect ratio on the heat transfer function; $W/H = 4.65$–12 (118 data points of 20 plates). (d) Effect of the relative roughness pitch on the heat transfer function (60 data points of 9 plates). (e) Final heat transfer correlation. (f) Comparison of the experimental heat transfer function with the heat transfer function calculated from equations (23) and (24).

ened rods. They report the minimum of the heat transfer function at roughness Reynolds number values of 10–30. A similar variation of the heat transfer function with the roughness Reynolds number has been observed in the present investigation with the minimum at roughness Reynolds number of about 20.

9. Conclusions

This study has presented experimental results for flow of air in rectangular ducts of various aspect ratios with repeated transverse rib roughness on one broad wall, which is subjected to uniform heat flux. The effect of relative roughness height, relative roughness pitch, rib head chamfer angle, and duct aspect ratio on the friction factor and the heat transfer coefficient has been studied for flow Reynolds numbers of about 3000–20 000 (roughness Reynolds numbers, e^+, from 5 to 60). The main findings of the study are:

(1) As compared to the smooth duct, the presence of ribs at one broad wall of the duct yields up to about two-fold and three-fold increase in the Stanton number and the friction factor, respectively, for the range of Reynolds numbers (3000–20 000), chamfer angle (-15–$+18^\circ$), relative roughness height (0.014–0.033), relative roughness pitch (4.6–8.5) and duct aspect ratio (4.65–12) investigated.
(2) The highest heat transfer and also the highest friction factor occur for 15° chamfered ribs.
(3) The duct aspect ratio has a strong effect on the heat transfer coefficient and the friction factor for a roughened rectangular duct.
(4) The value of the Stanton number is also found to be the function of both the relative roughness height and the Reynolds number. The roughness Reynolds number can be taken as a single dimensionless parameter combining the relative roughness height and the Reynolds number. The Stanton number first increases sharply with the increase in the roughness Reynolds number and then either decreases marginally or takes nearly constant value. The maxima of the Stanton number for cases with different flow and roughness geometries is found to occur at the roughness Reynolds number of about 20–25. It may be noted that the maxima in the Stanton number is also reported to occur at roughness Reynolds number of 25 for repeated rib in circular tubes [32] and for wire roughness in rectangular ducts [31].
(5) Based on the heat momentum transfer analogy, the friction and the heat transfer correlations have been developed which are valid for $3000 \leqslant Re \leqslant 20\,000$, $0.0141 \leqslant e/D_h \leqslant 0.0328$, $4.58 \leqslant p/e \leqslant 8.54$, $0^\circ \leqslant \phi \leqslant 15^\circ$ and $4.65 \leqslant W/H \leqslant 12$ with corresponding roughness Reynolds number of about 7–60.
(a) The roughness function is found to be independent of the roughness Reynolds number for values of the roughness Reynolds number greater than 20. The result is in agreement with Webb [17] and Han et al. [4] who reported this value as 25 and 35 for repeated rib roughness in tubes and rectangular ducts, respectively, unlike the value of 55–70 for sand grain roughness [2, 41].
(b) The minima of the heat transfer function occurs at roughness Reynolds number of about 20. Dalle Donne and Meyer [17] report the minima of the function at the roughness Reynolds number of 10–30 for flow of air in circular annuli with roughened rods.
(c) The heat transfer function increases with the increase in the aspect ratio from 4.65 to 9.66, and the roughness function decreases with the increase in the aspect ratio from 4.65 to 7.75. Thereafter both the functions attain nearly a constant value.

References

[1] D. Gupta, S.C. Solanki, J.S. Saini, Heat and fluid flow in rectangular solar air heater ducts having transverse rib roughness on absorber plate, Solar Energy 51 (1) (1993) 31–37.
[2] J. Nikuradse, Laws of flow in rough pipes, NACA, Technical Memorandum 1292, November 1950.
[3] J.C. Han, J.S. Park, Developing heat transfer in rectangular channels with rib-turbulators, Int. J. Heat Mass Transfer 31 (1988) 183–195.
[4] J.C. Han, L.R. Glicksman, W.M. Rohsenow, An investigation of heat transfer and friction for rib-roughened surfaces, Int. J. Heat Mass Transfer 21 (1978) 1143–1156.
[5] J.C. Han, J.S. Park, C.K. Lei, Augmented heat transfer in rectangular channels of narrow aspect ratios with rib turbulators, Int. J. Heat Mass Transfer 32 (1989) 1619–1630.
[6] J.C. Han, Y.M. Zhang, C.P. Lee, Augmented heat transfer in square channel with parallel, crossed, and V-shaped angled ribs, Journal of Heat Transfer 113 (1991) 590–596.
[7] R.L. Webb, E.R.G. Eckert, R.J. Goldstein, Heat transfer and friction in tubes with repeated rib-roughness, Int. J. Heat Transfer 14 (1971) 601–617.
[8] J.F. Lockett, M.W. Collins, Holographic interferometry applied to rib-roughness heat transfer in turbulent flow, Int. J. Heat Transfer 33 (1990) 2439–2449.
[9] D.F. Dipprey, R.H. Sabersky, Heat and momentum transfer in smooth and rough tubes at various Prandtl numbers, Int. J. Heat Mass Transfer 6 (1963) 329–353.
[10] F. Williams, M.A.M. Pirie, C. Warburton, Heat transfer from surfaces roughened by ribs, in: A. Bergles, R.L. Webb (Eds.), Augmentation of Heat Transfer, ASME, New York, 1970, pp. 36–43.
[11] F. Williams, J. Watts, The development of rough surfaces with improved heat transfer performance and a study of

mechanisms involved, Proceedings of the 4th International Heat Transfer Conference, Paris 2 (FC 5.5) (1970) 1–11.
[12] B.N. Prasad, J.S. Saini, Effect of artificial roughness on heat transfer and friction factor in a solar air heater, Solar Energy 41 (6) (1988) 555–560.
[13] D. Wilkie, Forced convection heat transfer from surfaces roughened by transverse ribs, Proceedings of the 3rd International Heat Transfer Conference, Chicago 1 (1996) 1–19.
[14] D. Wilkie, L. White, Calculation of flow resistance of passages bounded by a combination of rough and smooth surfaces, UKAEA Trg. Report 1113(W), 1965.
[15] E.M. Sparrow, L.M. Hossfeld, Effect of rounding of protruding edges on heat transfer and pressure drop in a duct, Int. J. Heat Mass Transfer 36 (1993) 147–153.
[16] T.M. Liou, J.J. Hwang, Effect of ridge shapes on turbulent heat transfer and friction in a rectangular channel, Int. J. Heat Mass Transfer 36 (1993) 931–940.
[17] M. Dalle Done, L. Meyer, Turbulent convective heat transfer from rough surfaces with two-dimensional rectangular ribs, Int. J. Heat Mass Transfer 20 (1977) 583–620.
[18] R. Sethumadhavan, M. Raja Rao, Turbulent flow heat transfer and fluid friction in helical-wire-coil inserted tubes, Int. J. Heat Mass Transfer 26 (1983) 1833–1845.
[19] J.C. Han, Heat transfer and friction in channels with two opposite rib-roughened walls, Journal of Heat Transfer 106 (1984) 774–781.
[20] E.M. Sparrow, W.Q. Tao, Enhanced heat transfer in a flat rectangular duct with streamwise-periodic disturbances at one principal wall, Journal of Heat Transfer 105 (1993) 851–861.
[21] Y.-D. Liu, L.A. Diaz, N.V. Suryanarayana, Heat transfer enhancement in air heating flat plate solar collectors, Journal of Solar Energy Engineering 106 (1984) 358–363.
[22] T.M. Liou, J.J. Hwang, Turbulent heat transfer augmentation and friction in periodic fully developed channel flow, Journal of Heat Transfer 114 (1992) 56–63.
[23] A.E. Bergles, Some perspective on enhanced heat transfer—second generation heat transfer technology, Journal of Heat Transfer 110 (1988) 1082–1096.
[24] ASHRAE Standard 93-77, Methods of testing to determine the thermal performance of solar collectors, New York, 1977.
[25] S.J. Kline, F.A. McClintock, Describing uncertainties in single sample experiments, Mechanical Engineering 75 (1953) 3–8.
[26] V. Gnielinski, New equations for heat and mass transfer in turbulent pipe and channel flow, International Chemical Engineering 16 (1976) 359–368.
[27] M.S. Bhatti, R.K. Shah, Turbulent and transition flow convective heat transfer, in: S. Kakac, R.K. Shah, W. Aung (Eds.), Handbook of Single-Phase Convective Heat Transfer, Chap. 4, John Wiley and Sons, New York, 1987.
[28] E.M. Sparrow, J.R. Lloyd, C.W. Hixon, Experiment on turbulent heat transfer in an asymmetrically heated rectangular duct, Journal of Heat Transfer 88 (1966) 170–174.
[29] J.L. Novotny, S.T. McComas, E.M. Sparrow, E.R.G. Eckert, Heat transfer for turbulent flow in rectangular ducts with two heated and two unheated walls, AIChE Journal 10 (1964) 466–470.
[30] H.M. Tan, W.W.S. Charters, An experimental investigation of forced-convective heat transfer for fully-developed turbulent flow in a rectangular duct with asymmetric heating, Solar Energy 13 (1970) 121–125.
[31] D. Gupta, Investigations on fluid flow and heat transfer in solar air heaters with roughened absorbers, Ph.D. Thesis, University of Roorkee, Roorkee, India, 1993.
[32] R.L. Webb, Towards a common understanding of the performance and selection of roughness for forced convection, in: J.P. Hartnett et al. (Eds.), Handbook of Studies in Heat Transfer: A Festschrift for E.R.G. Eckert, Hemisphere, Washington, 1979, pp. 257–272.
[33] J.C. Han, J.S. Park, C.K. Lei, Heat transfer enhancement in channels with turbulence promoters, Journal of Engineering for Gas Turbines and Power 107 (1985) 628–635.
[34] N. Sheriff, P. Gumley, J. France, Heat transfer characteristics of roughened surfaces, UKAEA Trg. Report 447(R), 1963.
[35] N. Sheriff, P. Gumley, Heat transfer and friction properties of surfaces with discrete roughnesses, Int. J. Heat Mass Transfer 9 (1966) 1297–1320.
[36] J.V. Vilemas, V.M. Simonis, Heat transfer and friction of rough ducts carrying gas flow with variable physical properties, Int. J. Heat Mass Transfer 28 (1985) 59–68.
[37] T.B. Burgoyne, P. Burnett, D. Wilkie, Force convection heat transfer from surfaces roughened by transverse ribs, UKAEA Trg. Report 781(W), 1964.
[38] P.M. Ligrani, R.J. Moffat, W.M. Kays, Artificially thickened turbulent boundary layers for studying heat transfer and skin friction on rough surfaces, J. Fluid Engineering 105 (1983) 146–153.
[39] A. Pedisius, A. Slanciauskas, Heat transfer in the transitional flow regime over surface roughness, Proc. 9th Int. Heat Transfer Conference, 3 (1990) 357–362.
[40] M.J. Lewis, Roughness functions, the thermohydraulic performance of rough surfaces and the Hall transformation—an overview, Int. J. Heat Mass Transfer 17 (1974) 809–814.
[41] P.R. Bandyopadhyay, Rough-wall turbulent boundary layers in the transition regime, J. Fluid Mech. 180 (1987) 231–266.